Supplementary Material: Characterization of Dependencies Between Growth and Division in Budding Yeast

Michael B. Mayhew
Computational Engineering Division, Lawrence Livermore National Laboratory
Livermore, CA USA

Edwin S. Iversen
Department of Statistical Science, Duke University
Durham, NC USA

Alexander J. Hartemink
Department of Computer Science &
Program in Computational Biology & Bioinformatics, Duke University
Durham, NC USA

February 16, 2017

1 Single-cell measurements of *Saccharomyces cerevisiae* growth and division

Single-cell haploid yeast data from 26 wild-type lineages (213 cells), 19 6×CLN3 lineages (99 cells) growing in glucose and 21 wild-type lineages (157 cells) growing in glycerol/ethanol described in [1] were kindly provided by the authors of that study. To track mass accumulation for each cell, the promoter of the constitutively expressed gene ACT1 was inserted upstream of the coding sequence of the red fluorescent protein, DsRed [1]. This construct was inserted once into the genome at the TRP1 locus (in the case of wild-type cells) or twice at the URA3 locus (in the case of 6×CLN3 cells). Endogenous ACT1 was not deleted in the strains used. When ACT1 was transcribed, both endogenous ACT1 and DsRed protein were expressed. Total protein is continuously synthesized in budding yeast. Due to the constitutive expression of ACT1 (and assuming good correlation between gene and protein expression), total DsRed fluorescence in each cell was used as a proxy for total protein or mass. Images were taken of wild-type and 6×CLN3 cells every 3 minutes while images of cells growing in glycerol/ethanol were taken every 6 minutes. The background fluorescence value of 199.0 was subtracted from the total DsRed fluorescence values for each cell. Background-subtracted total DsRed fluorescence for each cell was then normalized by the average (background-subtracted) total DsRed fluorescence at budding in each microcolony. Each microcolony corresponds to one lineage with the exception of one wild-type microcolony in glucose that mapped to two lineages. Normalized masses were used in all subsequent analyses of cell size. Thirteen wild-type cells grown in glycerol/ethanol did not have recorded masses but did have budding and division measurements. These cells were excluded from all analyses involving size. We refer interested readers to that article and its accompanying supplement for relevant details about strain construction and experimental protocols.

For our analysis on the effect of differences in size at budding on differences in $S/G_2/M$ duration and our Bayesian regression analysis we used a subset of cells in each lineage to control for autocorrelation in cell-cycle progression and to prevent double-counting of daughter cycles as mothers. For mother cells, we only retained mother data from 'leaves' of each lineage tree, and, if a mother underwent multiple prior cell cycles, we retained every other cycle, starting with the 'leaf' cycle. For daughter cells, we retained all daughter cycles. This procedure resulted in our subset of mother (wt, glucose N=78; 6×CLN3 N=35; wt, gly/eth N=58) and daughter (wt, glucose N=70; 6×CLN3 N=34; wt, gly/eth N=44) cells. Scatterplots of cell-cycle and growth characteristics for these cells are shown in Figures 1, 2, 3, 4, 5, and 6.

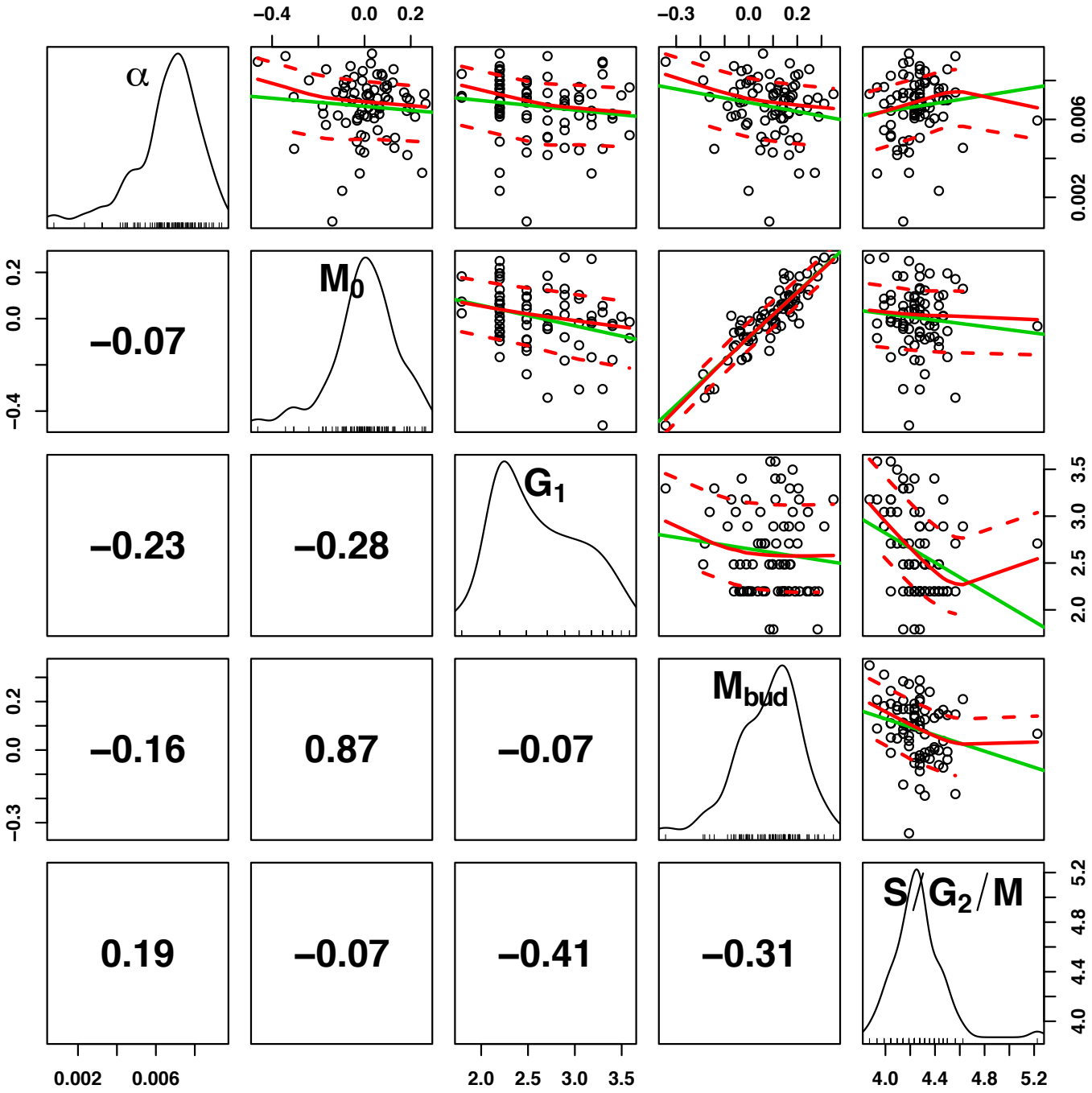

Figure 1: Scatterplots of observed cell-cycle durations and cell growth measurements in wild-type mothers (glucose). Shown along the diagonal are marginal distributions of estimated mass accumulation rates (α), observed masses at birth (M_0) and budding (M_{bud}), and observed cell-cycle durations for G_1 and $S/G_2/M$. The cell-cycle durations are on the natural logarithmic scale. In the lower diagonal are Spearman rank correlation coefficients and, in the upper diagonal, appear scatterplots for each pairwise relationship. Linear least-squares fit lines (green), loess smoothed fit lines (red solid), and loess variability bounds (red dashed) also appear in the upper diagonal plots.

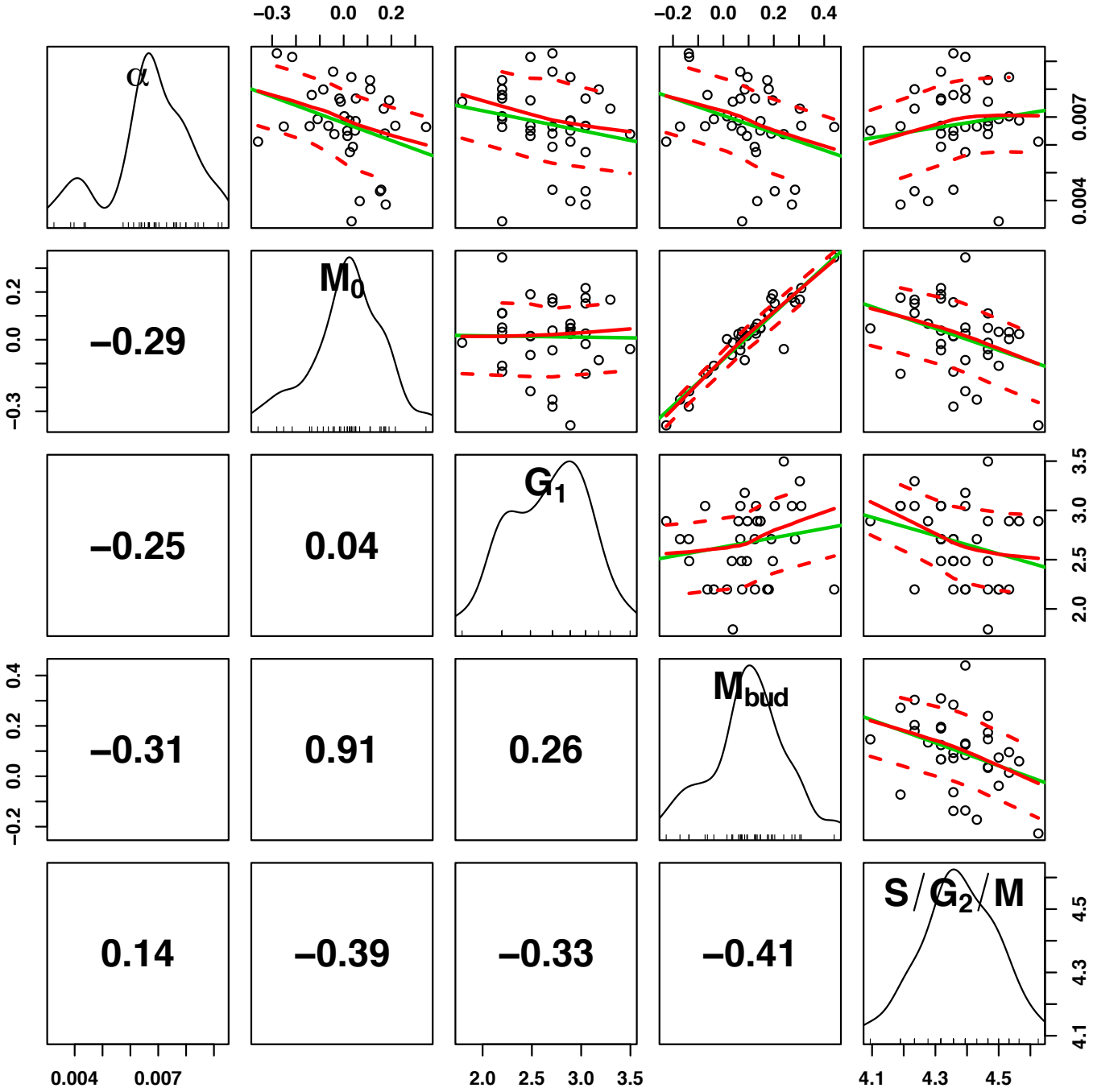

Figure 2: Scatterplots of observed cell-cycle durations and cell growth measurements in 6×CLN3 mothers. Layout is as in Figure 1.

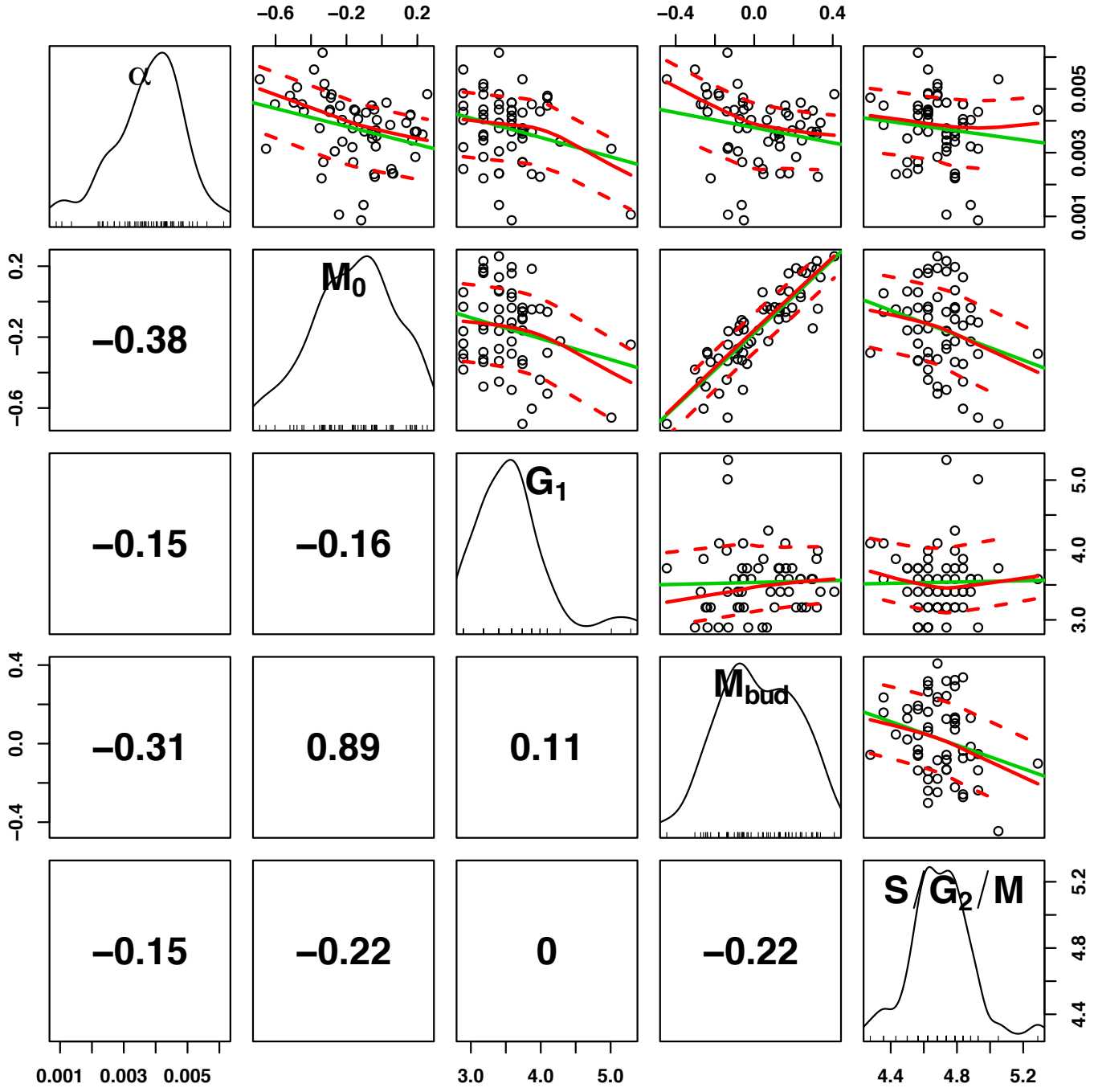

Figure 3: Scatterplots of observed cell-cycle durations and cell growth measurements in wild-type mothers (glycerol/ethanol). Layout is as in Figure 1.

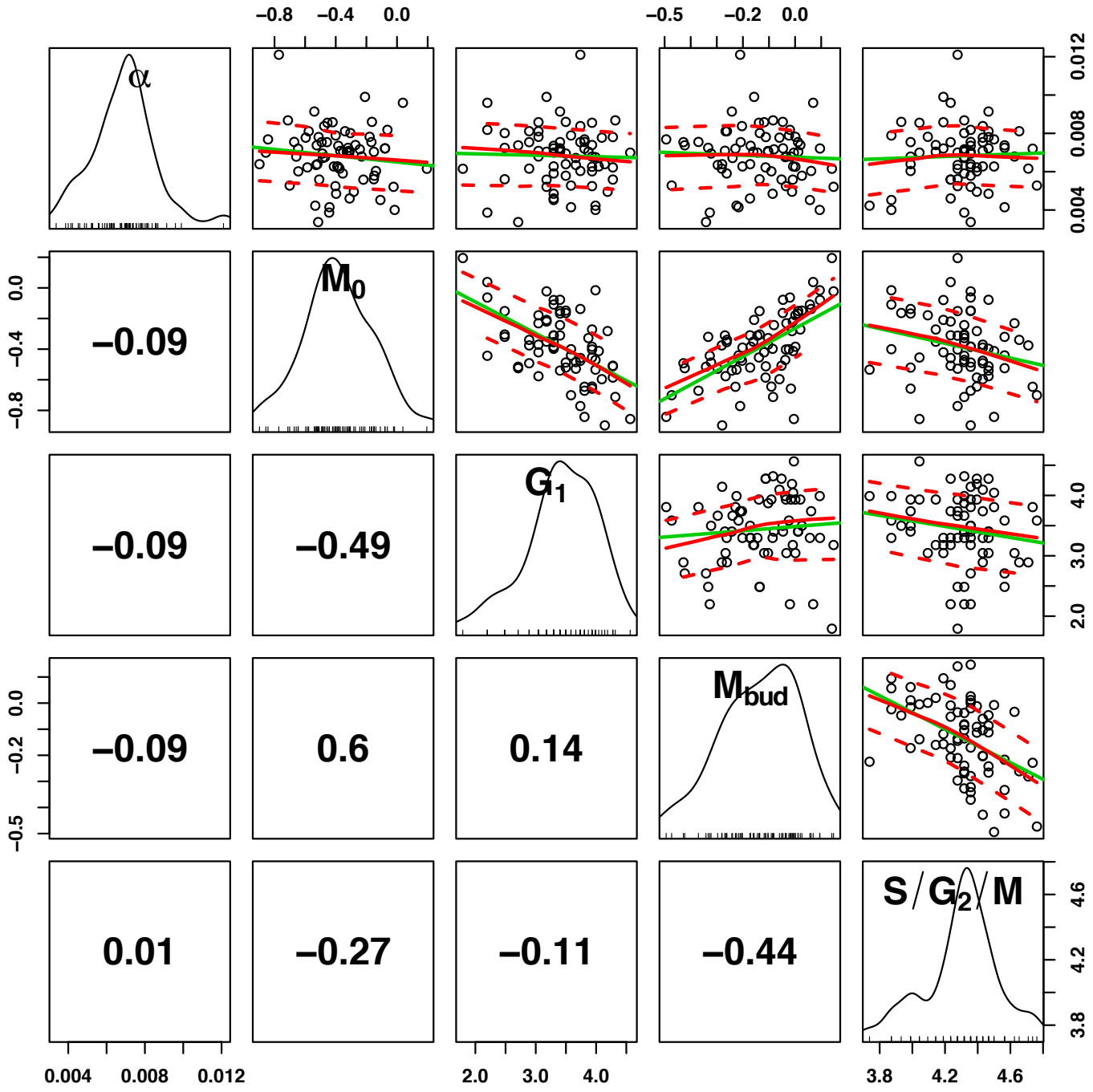

Figure 4: Scatterplots of observed cell-cycle durations and cell growth measurements in wild-type daughters (glucose). Layout is as in Figure 1.

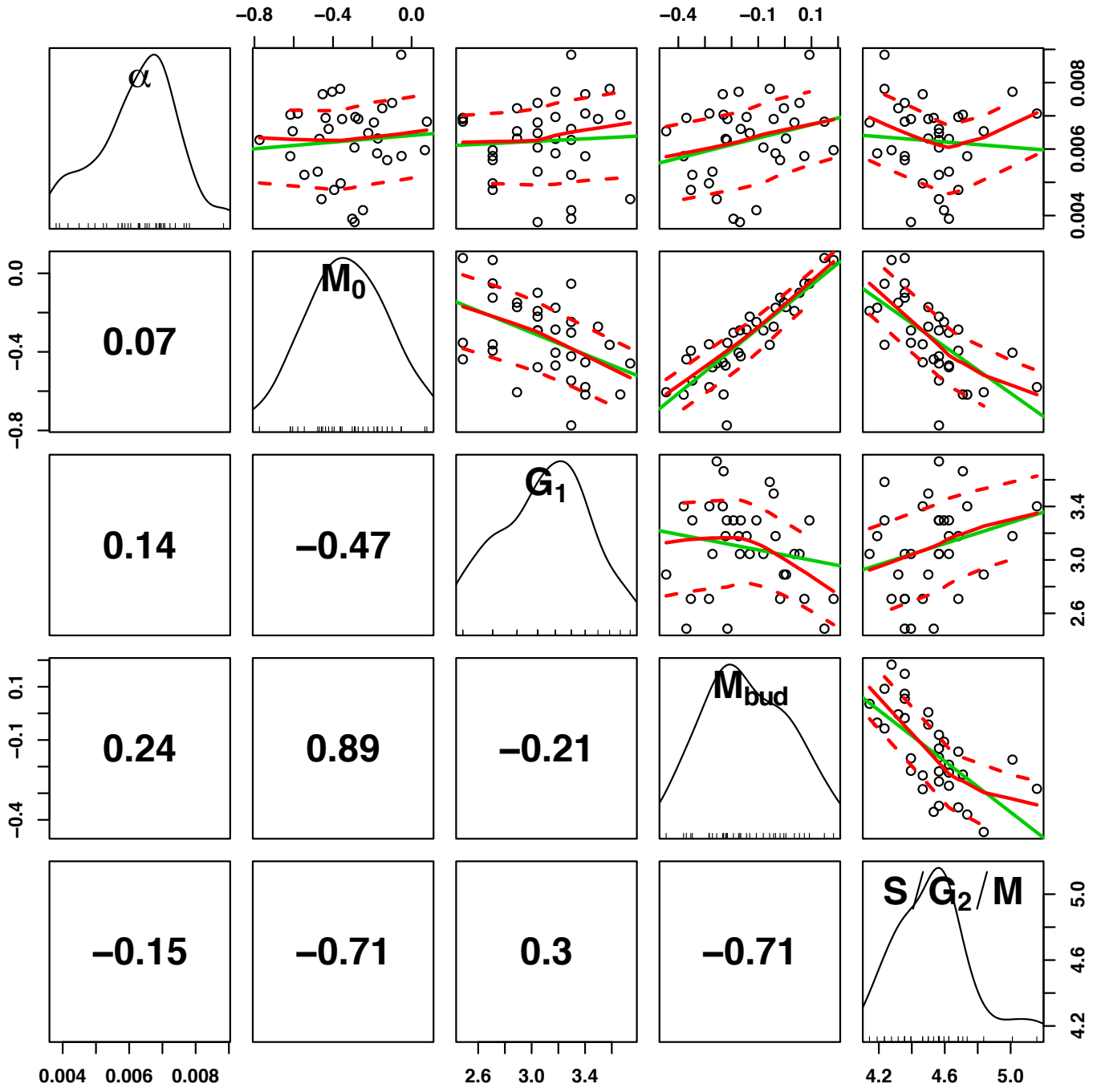

Figure 5: Scatterplots of observed cell-cycle durations and cell growth measurements in 6×CLN3 daughters. Layout is as in Figure 1.

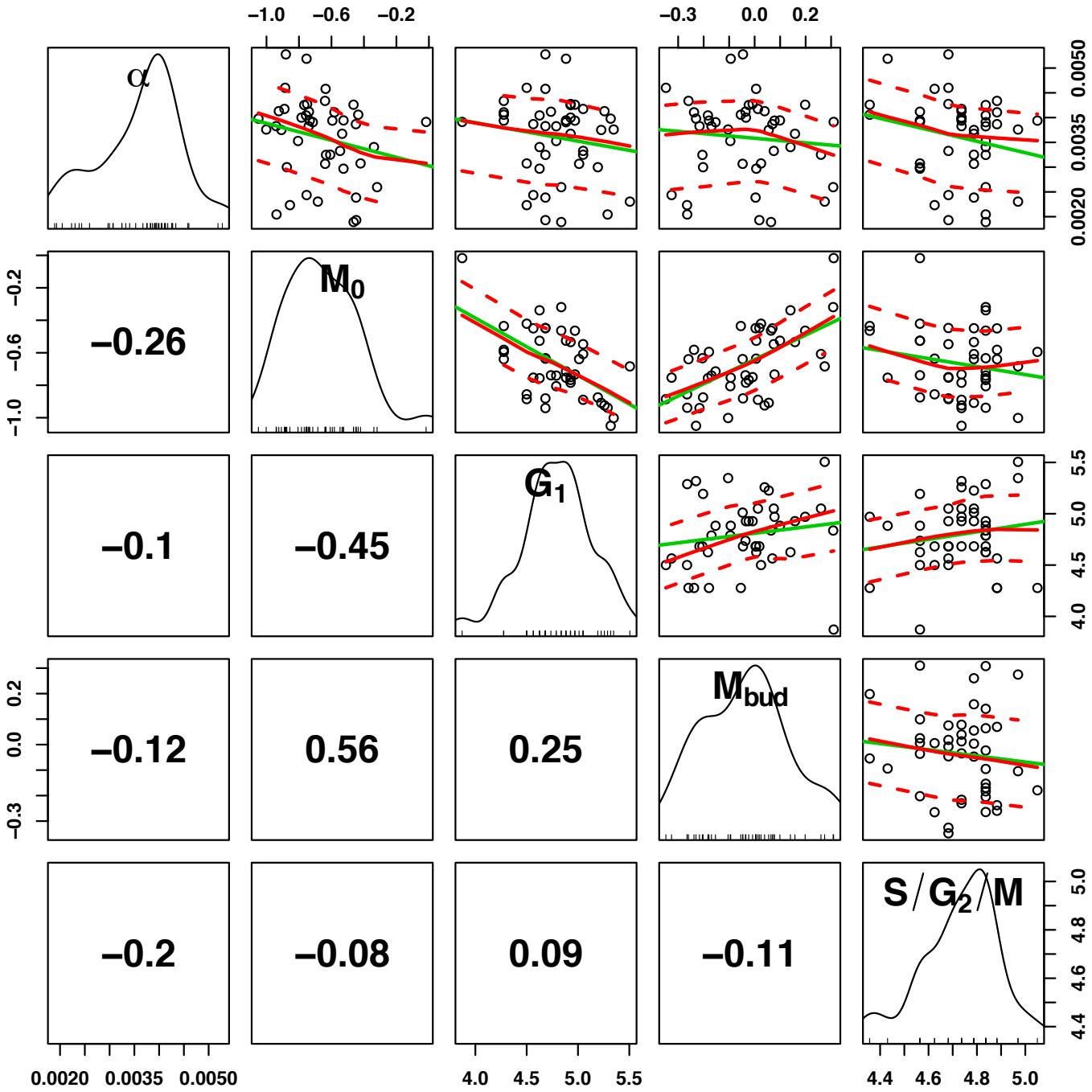

Figure 6: Scatterplots of observed cell-cycle durations and cell growth measurements in wild-type daughters (glycerol/ethanol). Layout is as in Figure 1.

	Wild-Type Glucose		6×CLN3 Glucose		Wild-Type Gly/Eth	
Parameter	**Estimate**	**(P-value)**	**Estimate**	**(P-value)**	**Estimate**	**(P-value)**
μ_{diff}	-0.26	(1.03×10^{-6})	-0.06	(0.366)	0.09	(0.068)
$w_{M_{B,diff}}$	-1.16	(2.19×10^{-8})	-0.68	(0.047)	-0.36	(0.061)

Table 1: Effect of daughter-mother differences in size at budding on differences in log S/G_2/M duration. Shown are parameter estimates with p-values assessing whether estimates were significantly different from 0 (in parentheses). P-values less than 0.001 are shown in scientific notation.

2 Estimating cell sizes and cell-specific growth characteristics

To estimate a cell's size at birth and budding as well as its growth rate, we first assumed exponential single-cell growth kinetics.

$$M_t = M_0 e^{\alpha t} \tag{1}$$

The masses M_t are the normalized counts of total red fluorescence (background-subtracted) in the cell at time t in the time-lapse movie. Paired with a cell's vector of masses is the cell's 'time vector', $\tilde{t}_{i,j}$. $\tilde{t}_{i,j}$ is the vector of time points (in minutes) at which the mass observations were taken (e.g., {0,3,6,...}). With a cell's mass and time vectors, we fit the following linear model to estimate mass accumulation rates and birth masses:

$$\mathsf{log}(M_{i,j,k}) = \mathsf{log}(M_{0,i,j}) + \alpha_{i,j} \cdot t_{i,j,k} + \epsilon \tag{2}$$

We assume ϵ is a normally distributed error term with zero mean and unit variance. ϵ is also assumed identically and independently distributed with respect to time. $M_{i,j,k}$ and $t_{i,j,k}$ are the kth elements of cell j's mass and time vectors, respectively. $\mathsf{log}(M_{0,i,j})$ or $\hat{M}_{0,i,j}$ is the intercept of this linear model and $\alpha_{i,j}$ is the slope. The fitted mass at budding ($\hat{M}_{B,i,j}$) was also estimated by the following:

$$\hat{M}_{B,i,j} = \hat{M}_{0,i,j} + \hat{\alpha}_{i,j} \cdot t_{i,j,B} \tag{3}$$

where $t_{i,j,B}$ is the time of budding for cell j. Estimates of $\hat{M}_{0,i,j}$, $\hat{M}_{B,i,j}$, and $\hat{\alpha}_{i,j}$ were retained for subsequent analysis of the connections between growth and division (with the 'hat' symbol dropped in figures of the main manuscript).

3 Effect of mother-daughter differences in cell size on differences in log S/G_2/M progression

We tested the hypothesis that mother-daughter differences in log S/G_2/M duration were associated with differences in cell size. We first paired all mothers with their first daughters for the three datasets (wild-type in glucose: 44 pairs; 6×CLN3: 16 pairs; wild-type in glycerol/ethanol: 26 pairs). We then computed the differences in daughter and mother masses at budding ($\hat{M}_{B,\mathit{diff}}$) and S/$G_2$/M durations. Finally, we fit a linear regression of daughter-mother difference in log S/G_2/M duration (S_{diff}) on differences in mass at budding.

$$S_{\mathit{diff}} = \mu_{\mathit{diff}} + w_{M_{B,\mathit{diff}}} \hat{M}_{B,\mathit{diff}} + \epsilon \tag{4}$$

In two of the three experimental settings (wild-type in glucose: p-value=2.19×10^{-8}; 6×CLN3: p-value=0.047), the difference between daughter and mother mass at budding was a significant predictor of differences in S/G_2/M duration (Table 1). In wild-type in glycerol/ethanol, the difference between daughter and mother mass at budding was a suggestive but not significant predictor (p-value=0.061). Estimates for the coefficient of mass at budding were also consistent with what one might expect from G_1 size dependence: a daughter cell larger at budding than its mother tends to have a comparatively shorter S/G_2/M duration (Table 1). Interestingly, the estimate for μ_{diff} was significantly different from 0 for wild-type cells in glucose, suggesting that daughter-mother S/G_2/M differences could not be explained solely by size differences in this condition. Conversely, differences in 6×CLN3 and wild-type (in glycerol/ethanol) S/G_2/M duration were largely explained by differences in size as the corresponding estimate for μ_{diff} did not differ significantly from 0 (Table 1). In contrast to our results for mother-daughter S/G2/M differences (part B of section II), we find that S/G_2/M duration for wild-type daughters in glucose is shorter compared with mother durations (μ_{diff} estimate in Table 1). This result is likely due to the fact that we are conditioning on the strongly predictive size differences which are correlated with the baseline differences in S/G_2/M duration. In our

first analysis of $S/G_2/M$ differences in part B of section II, we were only considering $S/G_2/M$ without accounting for effects of differences in size. These findings not only suggest that $S/G_2/M$ duration can vary between mother and daughter cells but that daughters tend to spend more time in the budded state than mothers, and differences in mass at budding help explain this difference in $S/G_2/M$ duration.

4 Assessing effect of cell growth characteristics on cell division

We used a Bayesian model averaging approach (Bayesian adaptive sampling [11]; R package BAS) to evaluate possible models of dependence between growth and division. We considered 7 different explanatory variables, and the set of all possible subsets of these explanatory variables comprises $2^7 = 128$ possible models. We assume that each model is equally plausible *a priori*. With this assumption and the relatively small number of possible models, posterior probabilities of each model can be computed straightforwardly and exactly. To induce shrinkage of regression coefficients towards 0, we place a hyper-g prior on the shrinkage parameter g with the corresponding a parameter set to 3 [12].

The full regression model is as follows:

$$\begin{aligned} S_{i,j} = \mu_S + w_{S_{Pa}} S_{i,Pa(j)} + w_\alpha \hat{\alpha}_{i,j} + w_{M_0} \hat{M}_{0,i,j} + w_{M_B} \hat{M}_{B,i,j} \\ + w_{\alpha_{Pa}} \hat{\alpha}_{i,Pa(j)} + w_{M_{0,Pa}} \hat{M}_{0,i,Pa(j)} + w_{M_{B,Pa}} \hat{M}_{B,i,Pa(j)} + \epsilon_{i,j}. \end{aligned} \tag{5}$$

μ_S is an intercept term and $S_{i,j}$ is the observed $S/G_2/M$ duration for a cell in its current cycle. $S_{i,Pa(j)}$ is the $S/G_2/M$ duration either of a cell in its previous cycle (for mothers) or of its mother's cycle (for daughters). The other explanatory variables of the linear model ($\hat{\alpha}_{i,j}$, $\hat{\alpha}_{i,Pa(j)}$, $\hat{M}_{0,i,j}$, $\hat{M}_{0,i,Pa(j)}$, $\hat{M}_{B,i,j}$, and $\hat{M}_{B,i,Pa(j)}$) are the aforementioned growth characteristics of cells. With the Bayesian adaptive sampling framework, we computed marginal posterior probabilities of each model for both mother cells (Figure 5 of main text) and daughter cells (Figure 6 of main text). Results of this analysis are described in Section II Part D of the main text.

5 Modeling budding yeast cell division at the single-cell level

We use a hierarchical framework to model budding and division durations and the correlations between them. In taking a Bayesian approach to parameter inference, we appeal to Bayes' theorem:

$$Pr(\Theta_{pop}, \tilde{\gamma}, \tilde{\beta}, \tau^2 \mid \tilde{B}^{rel}, \tilde{C}^{rel}) \propto \prod_{i=1}^{\mathcal{L}} Pr(\tilde{B}_i^{rel}, \tilde{C}_i^{rel} \mid \tilde{\gamma}_i, \tilde{\beta}_i, \tau^2, \Theta_{pop}) Pr(\tilde{\gamma}_i \mid \Theta_{pop}) Pr(\tilde{\beta}_i) Pr(\Theta_{pop}, \tau^2). \tag{6}$$

That is, the posterior distribution of model parameters is proportional to the product of the likelihood of the budding and division durations and the prior distribution on model parameters. The parameters of the hierarchical model are: $\tilde{\gamma}_i$, the vector of cell-specific branch lengths that give the expected values of observed budding and division durations; Θ_{pop}, the subset of population-level parameters $\{\Lambda, \Delta, \sigma_\lambda^2, \sigma_\delta^2, \psi, \rho, \phi\}$; $\tilde{\beta}_i$, the proportions of cells' λs during which the cell is unbudded; and τ^2, the variance of measurement error in budding and division durations. $\mathcal{L}$ is the number of lineage trees in a particular experimental setting, and lineages are assumed independent of one another. Development of the model begins with specification of a likelihood and error model for the budding and division durations of a particular lineage:

$$Pr(\tilde{B}_i^{rel}, \tilde{C}_i^{rel} \mid \tilde{\gamma}_i, \tilde{\beta}_i, \tau^2, \Theta_{pop}). \tag{7}$$

We then specify a branching process—and corresponding probability distribution—describing the dependence structure in cell-specific branch lengths that give the expected values of the observed durations:

$$Pr(\tilde{\gamma}_i \mid \Theta_{pop}). \tag{8}$$

We specify an independent prior distribution on proportions of baseline expected cell-cycle duration (a cell's λ) during which the cell is unbudded:

$$Pr(\tilde{\beta}_i). \tag{9}$$

Finally, we specify the prior for population-level parameters (and measurement error) in the model hierarchy:

$$Pr(\Theta_{pop}) Pr(\tau^2). \tag{10}$$

5.1 Error model for budding and division times and durations

For each cell j in lineage i, we observe the elapsed time from the start of the time-lapse experiment to when the cell buds ($B_{i,j}$) or divides ($C_{i,j}$). For the marginal distributions of these budding and division times, we assume:

$$B_{i,j} \sim \mathsf{Norm}(\mu_{B_{i,j}}, \tau^2) \tag{11}$$

and

$$C_{i,j} \sim \mathsf{Norm}(\mu_{C_{i,j}}, \tau^2). \tag{12}$$

Stacking these times into a vector:

$$\begin{pmatrix} \tilde{B}_i \\ \tilde{C}_i \end{pmatrix} \sim \mathsf{MVNorm}(\tilde{\mu}_i, \tau^2) \tag{13}$$

where $\tilde{B}_i$ and $\tilde{C}_i$ are vectors of budding and division times for lineage i and $\tilde{\mu}_i$ is a vector of corresponding means $\mu_{B_{i,j}}$ and $\mu_{C_{i,j}}$.

We transform times into durations $B^{\mathsf{rel}}_{i,j}$ and $C^{\mathsf{rel}}_{i,j}$ by subtracting the total time spent to reach the division that produced cell j. More formally:

$$B^{\mathsf{rel}}_{i,j} = B_{i,j} - C_{i,Pa(j)} \tag{14}$$

$$C^{\mathsf{rel}}_{i,j} = C_{i,j} - C_{i,Pa(j)} \tag{15}$$

where $C_{i,Pa(j)}$ is the division time of the cell in lineage i that is cell j's direct antecedent or parent (e.g. $Pa(110) = 11$).

After this linear transformation, the likelihood for budding and division durations for lineage i is:

$$\begin{pmatrix} \tilde{B}^{\mathsf{rel}}_i \\ \tilde{C}^{\mathsf{rel}}_i \end{pmatrix} \mid \tilde{\gamma}_i, \Theta_{\mathit{pop}}, \tilde{\beta}_i, \tau^2 \sim \mathsf{MVNorm}(A\tilde{\mu}_i, \tau^2 AA').$$

A is the linear transformation matrix (a sparse matrix whose only non-zero values are ones and negative ones) and $\tilde{\mu}_i$ is the vector of the mean budding and division times. As previously mentioned, it is assumed that the budding and division observations are independent of one another across lineages (hence the product in eq. 6).

The cell-specific branch lengths ($\tilde{\gamma}_i = A\tilde{\mu}_i$) are used to specify the expected value of budding and division durations. The manner in which the cell-specific branch lengths correlate with one another is given by an asymmetric branching process following a multivariate probability distribution. Given the cell-specific branch lengths that arise from the branching process, cell-specific unbudded proportions ($\tilde{\beta}_i$), the population parameters Θ_{pop}, and the cell type of each cell j, the expected value of the budding and division durations are specified as:

$$E[B^{\mathsf{rel}}_{i,j} \mid \tilde{\gamma}_i, \Theta_{\mathit{pop}}, \tilde{\beta}_i] = \begin{cases} \beta_{i,j}\lambda_{i,j} & \text{if } j \in \mathcal{M}_i \\ \delta_{i,j} + \beta_{i,j}\lambda_{i,j} & \text{if } j \in \mathcal{D}_i \end{cases} \tag{16}$$

$$E[C^{\mathsf{rel}}_{i,j} \mid \tilde{\gamma}_i, \Theta_{\mathit{pop}}, \tilde{\beta}_i] = \begin{cases} \lambda_{i,j} & \text{if } j \in \mathcal{M}_i \\ \delta_{i,j} + \lambda_{i,j} & \text{if } j \in \mathcal{D}_i \end{cases}. \tag{17}$$

Here, $\mathcal{M}_i$ and $\mathcal{D}_i$ are the sets of indices in lineage i of mother and daughter cells, respectively.

5.2 Formal description of the asymmetric autoregressive branching process

As the budding and division durations are positively valued, we assume that the branch lengths $\tilde{\gamma}_i$ follow a log-normal distribution:

$$\tilde{\gamma}_i = e^{\tilde{\gamma}^*_i}$$

where

$$\tilde{\gamma}^*_i \mid \Theta^*_{\mathit{pop}} \sim \mathsf{MVNorm}(\mu^*_{\tilde{\gamma}_i}, \Sigma^*_{\tilde{\gamma}_i}).$$

We modeled the cell-specific branch lengths as log-normally distributed instead of the observed budding and division durations for two reasons: 1) we don't expect observation errors to increase with duration and 2) we wanted to decompose sources of variation in budding and division durations into cell-to-cell variability and measurement error. Here, $\tilde{\gamma}^*_i$ and Θ^*_{pop} consist of parameters analogous to those in $\tilde{\gamma}_i$ and Θ_{pop} except that they are on the natural logarithmic scale.

The multivariate normal specification just above indicates that, for a given experimental setting, these branch lengths ($\lambda^*_{i,j}$s and $\delta^*_{i,j}$s) are marginally drawn from normal distributions:

$$\lambda^*_{i,j} \sim \mathsf{Norm}(\Lambda^*, \sigma^{2*}_\lambda) \tag{18}$$

and

$$\delta^*_{i,j} \sim \mathsf{Norm}(\Delta^*, \sigma^{2*}_\delta). \tag{19}$$

On the original scale, σ^2_λ and σ^2_δ represent variation in the $\lambda_{i,j}$s and $\delta_{i,j}$s, respectively, denoting cell-to-cell variability in cell-cycle progression. Λ is the average population-level base cell-cycle duration: the population expected cell-cycle duration for a mother cell. The population expected cell-cycle duration of a daughter cell can be longer. Δ represents the population mean daughter-specific cell-cycle extension that explains this difference.

In describing the dependence between branch lengths, we assume that the branch lengths of each new cell j are conditionally independent of the branch lengths of any previous cell in the lineage given the cell-cycle progression of the new cell's parent cell, $Pa(j)$ (a first-order autoregressive or AR(1) assumption). We also further assume that the branch lengths of cell j take a conditional normal distribution given the λ^* of the cell's mother (or $\lambda^*_{i,Pa(j)}$). In particular:

$$\delta^*_{i,j} \mid \lambda^*_{i,Pa(j)}, \Theta^*_{pop} \sim \mathsf{Norm}\Big(\Delta^* + \phi^*\Big(\frac{\sigma^*_\delta}{\sigma^*_\lambda}\Big)(\lambda^*_{i,Pa(j)} - \Lambda^*), (1-\phi^{2*})\sigma^{2*}_\delta\Big) \text{ for } j \in \mathcal{D}_i \tag{20}$$

$$\lambda^*_{i,j} \mid \lambda^*_{i,Pa(j)}, \Theta^*_{pop} \sim \mathsf{Norm}\Big((1-\rho^*)\Lambda^* + \rho^*\lambda^*_{i,Pa(j)}, (1-\rho^{2*})\sigma^{2*}_\lambda\Big) \text{ for } j \in \mathcal{D}_i \tag{21}$$

$$\lambda^*_{i,j} \mid \lambda^*_{i,Pa(j)}, \Theta^*_{pop} \sim \mathsf{Norm}\Big((1-\psi^*)\Lambda^* + \psi^*\lambda^*_{i,Pa(j)}, (1-\psi^{2*})\sigma^{2*}_\lambda\Big) \text{ for } j \in \mathcal{M}_i. \tag{22}$$

The above conditional normal assumptions lead to the joint multivariate normal specification given above for the branch lengths of lineage i conditional on the population parameters, Θ^*_{pop}:

$$\tilde{\gamma}^*_i \mid \Theta^*_{pop} \sim \mathsf{MVNorm}(\mu^*_{\tilde{\gamma}_i}, \Sigma^*_{\tilde{\gamma}_i}) \tag{23}$$

where, due to the AR(1) assumption,

$$\Sigma^{*,-1}_{\tilde{\gamma}_i,j,k} = 0 \text{ if } j \neq k, j \neq Pa(k) \text{ and } k \neq Pa(j). \tag{24}$$

In other words, branch lengths of cells that are not part of the same 'triad' (a given mother cycle, the subsequent mother cycle, and daughter cycle) are independent of one another given all other branch lengths in the lineage tree. It is also important to note that the daughter and second mother cycles within a triad are conditionally independent of one another given the first mother cycle.

To get parameter inferences on the original scale, we use the following conversions from multivariate log-normal theory [13]:

$$\Lambda^* = 2\mathsf{log}(\Lambda) - (1/2)\mathsf{log}(\sigma^2_\lambda + \Lambda^2)$$

$$\sigma^{2*}_\lambda = \mathsf{log}(\frac{\sigma^2_\lambda + \Lambda^2}{\Lambda^2})$$

$$\Delta^* = 2\mathsf{log}(\Delta) - (1/2)\mathsf{log}(\sigma^2_\delta + \Delta^2)$$

$$\sigma^{2*}_\delta = \mathsf{log}(\frac{\sigma^2_\delta + \Delta^2}{\Delta^2})$$

$$\psi^* = \frac{\mathsf{log}(\psi\frac{\sigma^2_\lambda}{\Lambda^2} + 1)}{\mathsf{log}(\frac{\sigma^2_\lambda + \Lambda^2}{\Lambda^2})}$$

$$\rho^* = \frac{\mathsf{log}(\rho\frac{\sigma^2_\lambda}{\Lambda^2} + 1)}{\mathsf{log}(\frac{\sigma^2_\lambda + \Lambda^2}{\Lambda^2})}$$

$$\phi^* = \frac{\mathsf{log}(\phi\frac{\sigma_\delta\sigma_\lambda}{\Delta\Lambda} + 1)}{\sqrt{\mathsf{log}(\frac{\sigma^2_\delta + \Delta^2}{\Delta^2})}\sqrt{\mathsf{log}(\frac{\sigma^2_\lambda + \Lambda^2}{\Lambda^2})}}.$$

6 Correlation between origin cell branches

Our assumption of a first-order autoregressive dependence structure coupled with the fact that the founder cell's full cell-cycle duration is unobserved induces correlation between the branch lengths of the mother and daughter origin cells of each sub-lineage (main manuscript, Figure 7). Thus, we model the λ^*s and δ^*s of the origin cells of each sub-lineage with a full joint distribution ($Pr(\lambda^*_{i,MO}, \lambda^*_{i,DO}, \delta^*_{i,DO})$) as follows:

$$\lambda^*_{i,j} \sim \mathsf{Norm}(\Lambda^*, \sigma^{2*}_\lambda) \text{ for } j \in \mathcal{MO}_i \tag{25}$$

$$\delta^*_{i,k} \mid \lambda^*_{i,j} \sim \mathsf{Norm}\Big(\Delta + (\psi^*\phi^* \frac{\sigma^*_\delta}{\sigma^*_\lambda}(\lambda^*_{i,j} - \Lambda^*), \sigma^{2*}_\delta(1 - (\psi^*\phi^*)^2)\Big) \text{ for } k \in \mathcal{DO}_i \text{ and } j \in \mathcal{MO}_i \tag{26}$$

$$\lambda^*_{i,k} \mid \delta^*_{i,k}, \lambda^*_{i,j} \sim \mathsf{Norm}\Bigg(\Lambda^* + \frac{\rho^*\phi^*(1-\psi^{2*})}{1-(\psi^*\phi^*)^2}\frac{\sigma_\lambda}{\sigma_\delta}(\delta^*_{i,k} - \Delta^*) + \frac{\psi^*\rho^*\frac{1-\phi^{2*}}{1-(\psi^*\phi^*)^2}}{}(\lambda^*_{i,j} - \Lambda^*),$$
$$\Big[\sigma^{2*}_\lambda \frac{1-(\psi^*\phi^*)^2 - \rho^{2*}(\phi^{2*} - 2(\phi^*\psi^*)^2 + \psi^{2*})}{1-(\psi^*\phi^*)^2}\Big]\Bigg) \text{ for } k \in \mathcal{DO}_i \text{ and } j \in \mathcal{MO}_i. \tag{27}$$

7 Cell-specific unbudded periods

Besides cell-to-cell variation in branch lengths ($\lambda_{i,j}$s and $\delta_{i,j}$s), variation in the proportion of λ cells spend in the unbudded state might also be expected. To address this possibility, we assign a parameter $\beta_{i,j}$ to each cell. $\beta_{i,j}$ takes a value between 0 and 1 and is the proportion of $\lambda_{i,j}$ during which cell j from lineage i is unbudded. We again use a hierarchical prior specification to tie these parameters across cells in a lineage. As the $\beta_{i,j}$s might differ between mother and daughter cells, we use different hierarchical priors depending on the cell's type. So:

$$\beta_{i,j} \sim \mathsf{Beta}(\mu_m\eta_m, (1-\mu_m)\eta_m) \text{ for } j \in \mathcal{M}_i \tag{28}$$

and

$$\beta_{i,j} \sim \mathsf{Beta}(\mu_d\eta_d, (1-\mu_d)\eta_d) \text{ for } j \in \mathcal{D}_i. \tag{29}$$

Here, μ_m and μ_d represent the expected proportions of λ spent in the unbudded state and η_m and η_d are the prior degrees of freedom for mothers and daughters, respectively. We discuss the prior distributions on the hyperparameters (μ_m, μ_d, η_m, and η_d) in the next section.

8 Prior distributions on model parameters

In adopting a fully Bayesian approach to parameter inference, we incorporated empirical knowledge of budding yeast cell division in prior distributions on different model parameters. Specifically:

$$\mu_m, \mu_d \sim \mathsf{Beta}(2.4, 17.6) \tag{30}$$

$$\eta_m, \eta_d \sim \mathsf{Gamma}(27.1, 1.4) \tag{31}$$

$$\Lambda \sim \mathsf{Norm}(78.2, 18.2^2) \tag{32}$$

$$\Delta \sim \mathsf{Norm}(55.0, 22.5^2) \tag{33}$$

$$\psi, \rho, \phi \sim \mathsf{Unif}(-1.0, 1.0) \tag{34}$$

$$\sigma_\delta^{-2}, \sigma_\lambda^{-2} \sim \mathsf{Gamma}(0.95, 4.48) \tag{35}$$

$$\tau^{-2} \sim \mathsf{Gamma}(4.08, 10.18). \tag{36}$$

Many of these priors were biologically motivated and made sufficiently weak so as to allow the data to overwhelm them. Priors on Λ and Δ were based on observations of these estimated quantities in previous work with cell populations [3, 4]. The priors are diffuse in that we allow for Λ to take values between 41.8 and 114.6 minutes and for Δ to take values between 10 and 100 minutes with $\sim$95% probability. The $\mathsf{Beta}(2.4, 17.6)$ priors on μ_m and μ_d indicate an *a priori* expectation that cells spend 12% of their λ branch durations in the unbudded state. Priors on the hyperparameters η_m and η_d reflect a belief that prior degrees of freedom are less than 30 with high probability ($\sim$0.99) The $\mathsf{Unif}(-1.0, 1.0)$ priors on the correlation parameters reflect the lack of strong *a priori* information with mean prior correlations of 0. The $\mathsf{Gamma}(0.95, 4.48)$ priors on the precision rather than the variance in G1 phase delays (σ_δ^2) and cell-cycle durations (σ_λ^2) reflect prior beliefs that the standard deviations of the cell-specific branch lengths are less than 15 and greater than 1 with high probability ($\sim$0.965). The $\mathsf{Gamma}(4.08, 10.18)$ prior on precision in measurements of budding and division ($\frac{1}{\tau^2}$) is based on the belief that measurements are approximately within 6 minutes of their true values.

9 Posterior computation and sampling by Markov Chain Monte Carlo

We fit the model to the single-cell data using JAGS or Just Another Gibbs Sampler ([5]; mcmc-jags.sourceforge.net). The program builds a Markov chain Monte Carlo (MCMC) sampler based on the dependencies between and distributional assumptions on variables in a graphical model. The first 10,000 iterations were counted as burn-in to allow the sampler to find modes of high posterior probability. The subsequent 250,000 iterations were retained for each parameter. The MCMC chain was initialized for each dataset with sample-based estimates of each parameter. As we did not directly observe Λ or Δ, we used sample estimates of the budded and unbudded durations of each cell's cell cycle, respectively. Likewise, we initialized σ_λ^2 and σ_δ^2 with the sample variances of the budded and unbudded cell-cycle durations. The initial points of the correlation parameter chains were the sample correlations between successive mother budded durations (ψ), mother and daughter budded durations (ρ), and mother budded and daughter unbudded durations (ϕ). For τ^2, we used the prior mean as the MCMC starting point.

To incorporate the cell-specific beta parameters, we needed to extend JAGS with a custom helper function called diag that took a vector of parameters as argument and returned a matrix with the vector argument as its diagonal. We used the excellent tutorial on JAGS extensions by Wabersich [6] to implement this helper function. Our modified version of JAGS is available upon request.

The number of samples for each parameter was sufficient to estimate the 2.5th quantile of each parameter's marginal posterior distribution to within a 0.01 margin error with 90% probability by the Raftery-Lewis convergence diagnostic ([7]; `cran.r-project.org/package=coda`).

10 Evidence for longer S/G_2/M duration in daughters from hierarchical model inferences

We find corroboration for our previous analysis of differences in S/G_2/M duration between mother and daughter cells: the estimates for μ_m and μ_d (expected unbudded proportions of mother and daughter λ's; Table V in main manuscript). We find that the expected mother budded period ($1 - \mu_m$) is mildly (4% of total cell-cycle duration) shorter than the daughter budded period in wild-type cells growing in glucose, with the posterior probability of $(1-\mu_m) < (1-\mu_d)$ being 0.981. In 6×CLN3 cells, this difference in budded duration increases with mothers showing a nearly 8% shorter average budded duration and the posterior probability of $(1 - \mu_m) < (1 - \mu_d)$ being 0.996. In glycerol/ethanol, differences between mother and daughter budded durations are less pronounced. Although evidence for daughters spending more time in the budded proportion of the cell cycle was still strong (posterior probability of $(1 - \mu_m) < (1 - \mu_d)$ being 0.892), daughters only took $\sim$3% longer in their budded durations than their mothers.

11 Validation of different models of correlation with leave-one-out cross-validation

Different values for the the correlation parameters we introduce (ρ, ψ, and ϕ) correspond to different types of dependence structure among the cell-specific branch lengths of the branching process. To determine what model of correlation was most likely *a posteriori*, we performed a leave-one-out cross-validation analysis, predicting the observed division duration of each left-out cell. Leaving out random cells from each lineage wouldn't reveal the utility of the correlation parameters since some cells (e.g. origin cells) don't depend on those parameters. So, we

collected all 'leaf' cells or cells at the leaves of each lineage tree from each dataset. If origin cells were collected (due to small lineage trees), these cells were removed from the leave-out set. This procedure produced 113 cells from wild-type in glucose, 52 cells from 6×CLN3 cells in glucose, and 76 cells from wild-type in glycerol/ethanol.

For each left-out cell, we removed the observed budding and division durations from the data and fit models by MCMC with the remaining data in which one or a combination of the correlation parameters were set to 0. We also fit the full model in which all three correlation parameters were allowed to vary for a total of eight models (up to three parameters to include $\Rightarrow 2^3 = 8$ total possible models). For each model fitting, we ran JAGS for 10k burn-in iterations and 50k total iterations. We thinned the retained parameter chains, keeping every 10th iteration for a final set of 4k samples. Among these parameter samples, we retained samples of the cell-specific branch length of the left-out cell j's mother ($\lambda^*_{i,Pa(j)}$), of Λ^* and σ^*_λ (also of Δ^* and σ^*_δ if the left-out cell was a daughter), of any varying correlation parameters (samples set to 0 if correlation parameter was not allowed to vary) and of the measurement error variance τ^2. These samples were used to generate samples of the left-out cell's branch length $\lambda_{i,j}$. These samples were then used to compute posterior samples of the conditional mean and variance of the normal distribution generating the left-out cell's division duration. These samples are samples of the parameters of the posterior predictive distribution for each left-out cell.

To evaluate the predictive accuracy of each model, we evaluated the density of the each left-out cell's observed division duration under the predictive normal distribution defined by each posterior sample of the left-out cell's conditional mean and variance. The rationale here is if the correlation parameters are helping explain variation in cell-specific branch lengths, dropping those parameters will reduce accuracy in predicting a left-out cell's division duration, reflected in a lower density under the predictive distribution. We then took the mean of predictive densities evaluated at each sample for each left-out cell to get a single value of the expected predictive density for a left-out cell under each model. We then computed the natural logarithm of these expected densities for each left-out cell and each model. This approach is similar in spirit to other Bayesian model selection methods based on the posterior predictive density [14, 15].

As we had log expected predictive density values for each left-out cell on each of the eight tested models, we performed a Wilcoxon paired rank sum test to evaluate whether the log density under one model was significantly different than the log density under the null model (where all correlation parameters are set to 0.0). We also computed 95% confidence intervals for these model differences. Results appear in Table 2. As expected, no significant differences in model log density (compared with a model with no correlation; $\psi = 0$, $\phi = 0$, $\rho = 0$) were observed for wild-type cells in glucose and 6×CLN3 cells. Conversely, and consistent with our previous analyses, we did observe significant differences in model log density for wild-type cells grown in glycerol/ethanol. In general, models in which ψ (mother-mother correlation) could vary showed significantly higher log density compared with the baseline zero-correlation model while models where ψ was fixed to 0 generally led to lower relative log density.

12 Modeling effects of age and time spent in culture on cell-cycle progression

Replicative age (the number of divisions undergone by a cell) is one potential source of variation in cell-cycle progression unaccounted for in our hierarchical model. If population average cell-cycle progression did have some dependence on replicative age, one might observe a correlation between mother and/or daughter cycles due solely to this drift. However, studies suggest that mean cell-cycle duration is roughly constant for at least the first 10 cycles of a cell's life [9, 10]. Furthermore, the probability of finding a cell of replicative age 10 or more is vanishingly small since the younger cells outnumber older ones in an exponentially growing population (see [10] and references therein). Thus, for our analysis, we did not consider replicative age a likely source of variation in cell-cycle progression.

However, population average cell-cycle duration might still depend on experimental factors. For example, cell-cycle progression might depend on the number of cycles a cell spends in culture or the amount of exposure to excitation light during fluorescence microscopy. Thus, we extended our hierarchical model to include potential technical sources of variation leading to drift in expected cell-cycle duration. Rather than assume a constant population average base cell-cycle duration (Λ^*; on natural logarithmic scale), we allowed expected cell-cycle duration to vary with time spent on the agar slab by both cohorts of cells (*cohort* time; Figure 7A) and individual cells (*cell* time; Figure 7B). We assigned culture times under the two different cases to each cell cycle in each lineage of the glycerol/ethanol dataset. In the case of *cell* time, a cell j's expected duration on the logarithmic scale ($\Lambda^*_{a_{i,j}}$) was indexed by the number of cycles spent by the cell on the slab since its birth ($a_{i,j}$). Mother origin cycles—being one cycle removed from the first cell on the slab—were assigned the value 2. All daughter and daughter origin cell cycles were assigned the value 1. This culture time was incremented for each successive cycle. For example, a daughter cell cycle would be assigned the value 1, her subsequent cycle would be assigned the value 2, and so on. Likewise, the cycle following the mother

Table 2: Wilcoxon rank sum test results and 95% confidence intervals for leave-one-out cross-validation analysis.

Dataset	**Model**	**Median log-Ratio** (95% CI)		**P-value**
WT (Glucose)	Full	−1.023	(−3.564,4.550)	0.902
	$\psi = 0$	0.627	(−1.838,7.009)	0.385
	$\phi = 0$	−0.647	(−2.893,1.914)	0.563
	$\rho = 0$	−0.567	(−2.147,4.803)	0.624
	$\psi = 0, \rho = 0$	0.468	(−1.297,5.377)	0.385
	$\psi = 0, \phi = 0$	1.537	(−0.954,4.379)	0.195
	$\rho = 0, \phi = 0$	−0.105	(−2.426,1.760)	0.830
	$\psi = 0, \rho = 0, \phi = 0$	0	(0,0)	NA
6xCLN3 (Glucose)	Full	0.024	(−5.383,3.521)	0.809
	$\psi = 0$	0.722	(−2.768,4.960)	0.492
	$\phi = 0$	1.747	(−2.020,3.982)	0.341
	$\rho = 0$	1.843	(−1.867,4.581)	0.314
	$\psi = 0, \rho = 0$	0.830	(−1.964,3.501)	0.575
	$\psi = 0, \phi = 0$	0.558	(−1.698,3.727)	0.475
	$\rho = 0, \phi = 0$	1.304	(−1.563,4.999)	0.319
	$\psi = 0, \rho = 0, \phi = 0$	0	(0,0)	NA
WT (Gly/Eth)	Full	16.601	(1.614,35.656)	0.036
	$\psi = 0$	−7.556	(−23.100,−5.209)	0.0001
	$\phi = 0$	25.065	(4.523,39.794)	0.016
	$\rho = 0$	9.266	(−4.905,22.555)	0.139
	$\psi = 0, \rho = 0$	−4.565	(−15.655,−1.399)	0.014
	$\psi = 0, \phi = 0$	−5.066	(−9.509,3.167)	0.233
	$\rho = 0, \phi = 0$	23.431	(7.930,34.727)	0.002
	$\psi = 0, \rho = 0, \phi = 0$	0	(0,0)	NA

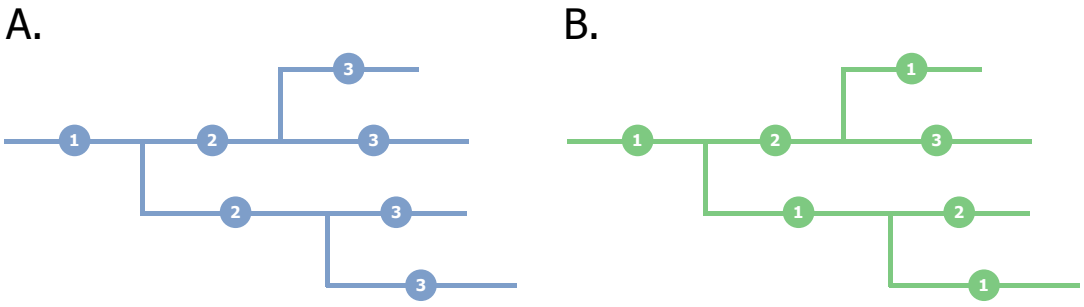

Figure 7: Lineage trees with two different codings of elapsed time in culture. In (A), integer values are assigned to cohorts of cells (cohort time) indicating the number of waves of division since the start of the time lapse experiment. So, the first cell observed is assigned the value 1, cells in the subsequent wave of division are assigned the value 2, etc. In (B), integer values are assigned to cycles of each cell, indicating the number of cycles that cell has spent in the culture environment. Thus, the first cell observed on the plate is assigned the value 1. Likewise, newborn cells receive the value 1. The second cycle of these cells is assigned the value 2, and so on.

origin's first cell cycle would be assigned the value 3, the subsequent cycle would take the value 4, etc. In the case of *cohort* time, we assigned indices ($a_{i,j}$) not to individual cell cycles but rather to the cycles of all cells in a particular wave of division. For instance, the cycle of the first cells in a lineage (either a mother origin or daughter origin's first cycle) would be assigned the value 1. At division, the mother or daughter origin cell would then produce a mother and a daughter, each assigned the value 2. Those cells would then produce mother and daughter cells with the value 3, and so on. We then augmented our cell division data with these elapsed time index assignments and fit the extended model (described in detail below) to the glycerol/ethanol data to infer time-specific expected cell-cycle durations (Λ_a; on the original scale).

Accounting for effects of culture times on population average cell-cycle duration involves some changes to the

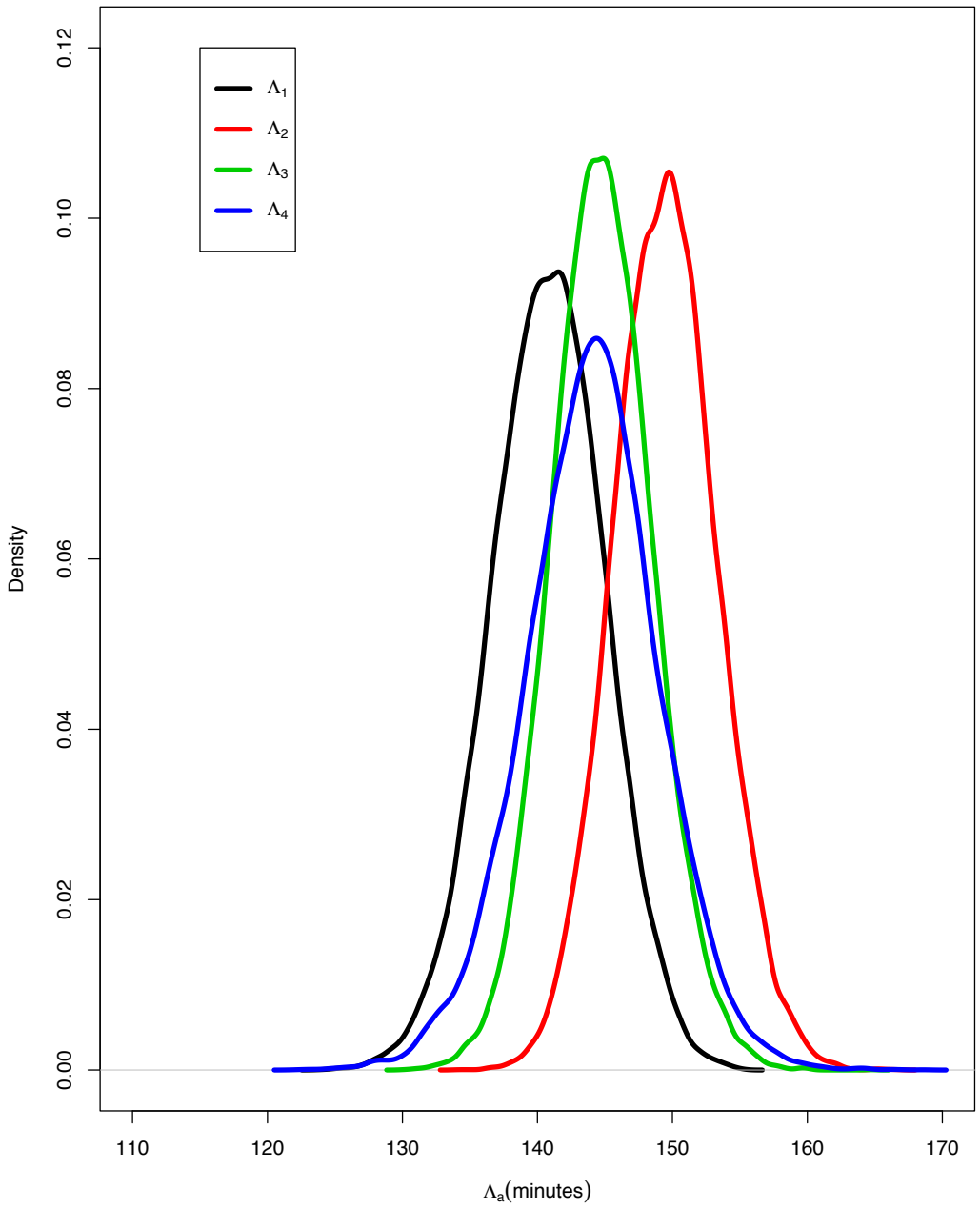

Figure 8: Shown are density estimates based on posterior samples of cell-time-specific Λ_as. The densities practically overlap one another and show no ordering with respect to elapsed time.

Table 3: Posterior inferences (modes and 95% highest posterior density intervals) for cell time-specific Λ_as

Parameter	Inferences
Λ_1	143.04 (119.14,151.05)
Λ_2	147.66 (140.62,155.53)
Λ_3	144.94 (135.93,152.63)
Λ_4	142.14 (132.24,151.00)
Λ_5	144.88 (133.87,156.53)

conditional and marginal specification for mother and daughter cell-specific $\lambda^*_{i,j}$'s.

$$\delta^*_{i,j} \mid \lambda^*_{i,Pa(j)}, \Theta^*_{\mathit{pop}} \sim \mathsf{Norm}(\Delta^* + \phi^*(\frac{\sigma^*_\delta}{\sigma^*_\lambda})(\lambda^*_{i,Pa(j)} - \Lambda^*_{a_{i,Pa(j)}}), (1-\phi^{2*})\sigma^{2*}_\delta) \text{ for } j \in \mathcal{D}_i \tag{37}$$

$$\lambda^*_{i,j} \mid \lambda^*_{i,Pa(j)}, \Theta^*_{\mathit{pop}} \sim \mathsf{Norm}(\Lambda^*_{a_{i,j}} + \rho^*(\lambda^*_{i,Pa(j)} - \Lambda^*_{a_{i,Pa(j)}}), (1-\rho^{2*})\sigma^{2*}_\lambda) \text{ for } j \in \mathcal{D}_i \tag{38}$$

$$\lambda^*_{i,j} \mid \lambda^*_{i,Pa(j)}, \Theta^*_{\mathit{pop}} \sim \mathsf{Norm}(\Lambda^*_{a_{i,j}} + \psi^*(\lambda^*_{i,Pa(j)} - \Lambda^*_{a_{i,Pa(j)}}), (1-\psi^{2*})\sigma^{2*}_\lambda) \text{ for } j \in \mathcal{M}_i. \tag{39}$$

$\Lambda^*_{a_{i,j}}$ and $\Lambda^*_{a_{i,Pa(j)}}$ are expected population baseline cell-cycle durations (on log scale) for cell j and its parent, indexed by the respective culture times of those cells ($a_{i,j}$ and $a_{i,Pa(j)}$). For example, if a mother cell j's cycle was assigned culture time equal to 4, its previous ($Pa(j)$) cycle would have culture time equal to 3. Thus, the conditional expectation for mother cell j's $\lambda^*_{i,j}$ parameter would be:

$$E[\lambda^*_{i,j}|\lambda^*_{i,Pa(j)}] = \Lambda^*_4 + \psi(\lambda^*_{i,Pa(j)} - \Lambda^*_3). \tag{40}$$

These model changes are also reflected in the distributions of $\lambda^*_{i,j}$'s for the mother and daughter origin cells:

$$\lambda^*_{i,j} \sim \mathsf{Norm}(\Lambda^*_{a_{i,j}}, \sigma^{2*}_\lambda) \text{ for } j \in \mathcal{MO}_i, \tag{41}$$

$$\delta^*_{i,k}|\lambda^*_{i,j} \sim \mathsf{Norm}\Big(\Delta + (\psi^*\phi^*\frac{\sigma^*_\delta}{\sigma^*_\lambda}(\lambda^*_{i,j} - \Lambda^*_{a_{i,j}}), \sigma^{2*}_\delta(1-(\psi^*\phi^*)^2)\Big) \text{ for } k \in \mathcal{DO}_i \text{ and } j \in \mathcal{MO}_i, \tag{42}$$

$$\lambda^*_{i,k}|\delta^*_{i,k}, \lambda^*_{i,j} \sim \mathsf{Norm}\Big(\Lambda^*_{a_{i,k}} + \frac{\rho^*\phi^*(1-\psi^{2*})}{1-(\psi^*\phi^*)^2}\frac{\sigma^*_\lambda}{\sigma^*_\delta}(\delta^*_{i,k} - \Delta^*) + \frac{\psi^*\rho^*(1-\phi^{2*})}{1-(\psi^*\phi^*)^2}(\lambda^*_{i,j} - \Lambda^*_{a_{i,j}}),$$
$$\Big[\sigma^{2*}_\lambda\frac{1-(\psi^*\phi^*)^2 - \rho^{2*}(\phi^{2*} - 2(\phi^*\psi^*)^2 + \psi^{2*})}{1-(\psi^*\phi^*)^2}\Big]\Big) \text{ for } k \in \mathcal{DO}_i \text{ and } j \in \mathcal{MO}_i. \tag{43}$$

Marginally:

$$\lambda^*_{i,j} \sim \mathsf{Norm}(\Lambda^*_{a_{i,j}}, \sigma^{2*}_\lambda). \tag{44}$$

To borrow strength for the estimates of these indexed parameters, we place a normal prior on the Λ_a's:

$$\Lambda_a \sim \mathsf{Norm}(\Lambda, \sigma^2_{a_\lambda}) \tag{45}$$

with

$$\Lambda^*_a = 2\mathsf{log}(\Lambda_a) - \frac{\mathsf{log}(\sigma^2_\lambda + \Lambda^2_a)}{2}. \tag{46}$$

We are effectively introducing a new layer in the model hierarchy between the asymmetric branching process parameters ($\tilde{\gamma}_i$) and the population-level parameters. For the variance parameter $\sigma^2_{a_\lambda}$, we expect *a priori* that variance in the time-specific means is similar to cell-to-cell variation in cell-cycle durations. Thus, we use a $\mathsf{Gamma}(0.95, 4.48)$ prior distribution.

Drift in mean base cell-cycle duration would be reflected in posterior inferences for the time-specific mean base cell-cycle durations (Λ_a): posterior confidence intervals for the parameters would not overlap one another or would be arranged in some order with respect to elapsed time. Our inferences under the two different elapsed time codings did not reveal obvious differences between the time-specific mean base cell-cycle durations (Figures 8 and 9; Tables 3 and 4). As such, these experimental factors are unlikely to explain the correlation in cell-cycle progression we see between successive mother cycles in glycerol/ethanol.

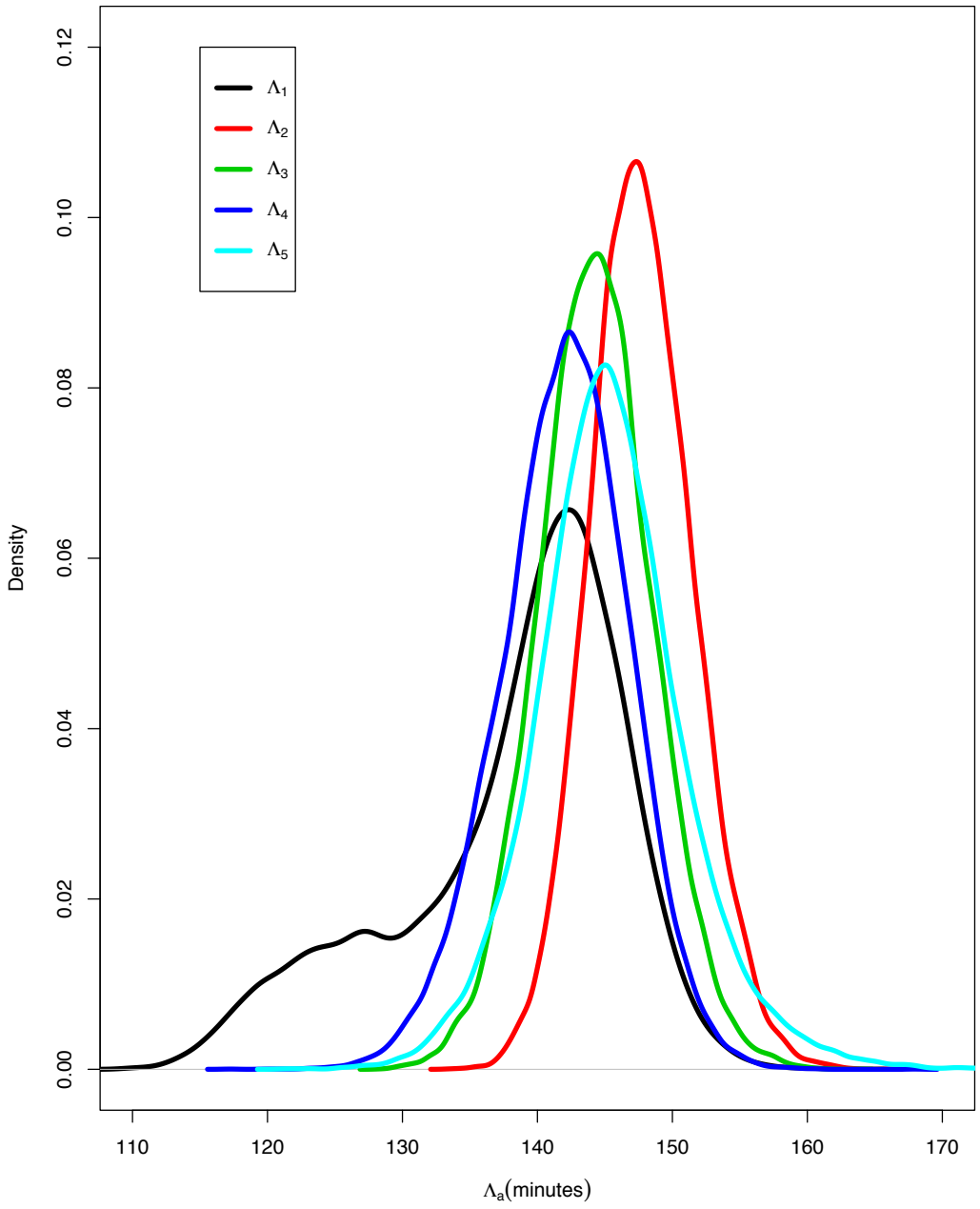

Figure 9: Shown are density estimates based on posterior samples of cohort-time-specific Λ_as. As in Figure 8, there is no obvious pattern in the Λ_a's.

Table 4: Posterior inferences (modes and 95% highest posterior density intervals) for cohort time-specific Λ_as

Parameter	**Inferences**
Λ_1	141.41 (132.69,149.12)
Λ_2	149.72 (142.26,157.13)
Λ_3	145.07 (137.64,152.30)
Λ_4	144.61 (134.10,153.79)

13 Acknowledgments

We would like to thank Stefano Di Talia and Frederick Cross; Sung Sik Lee and Matthias Heinemann for generously providing their data; and Merlise Clyde, Stefano Di Talia, Steve Haase, Daniel Lew, Nick Buchler, Bruce Futcher, Kurt Schmoller, Ivan Surovtsev, members of the Haase and Hartemink labs, and the anonymous reviewers for comments about the analysis and the manuscript. This work was funded in part by grants from NIH (P50 30 GM081883-01) and DARPA (HR0011-09-1-0040 to A.J.H.). This work was performed in part under the auspices of the U.S. Department of Energy by Lawrence Livermore National Laboratory under contract DE-AC52-07NA27344 (LLNL-JRNL-702334).

References

[1] Di Talia, S., Skotheim, J.M., Bean, J.M., Siggia, E.D., & Cross, F.R. 2007. The effects of molecular noise and size control on variability in the budding yeast cell cycle. *Nature*. **448**, 947-951. (DOI: 10.1038/nature06072)

[2] Johnston, G.C., Pringle, J.R., & Hartwell, L.H. 1977. Coordination of growth with cell division in the yeast *Saccharomyces cerevisiae*. *Exp Cell Res*. **105**, 79-98. (DOI: 10.1016/0014-4827(77)90154-9)

[3] Orlando, D.A., Iversen, E.S., Hartemink, A.J., & Haase, S.B. 2009. A branching process model for flow cytometry and budding index measurements in cell synchrony experiments. *Ann Appl Stat*. **3**, 1521-1541. (DOI: 10.1214/09-AOAS264)

[4] Mayhew, M.B., Robinson, J.W., Jung, B., Haase, S.B., Hartemink, A.J. 2011. A generalized model for multi-marker analysis of cell cycle progression in synchrony experiments. *Bioinformatics*. **27**, i295-i303. (DOI: 10.1093/bioinformatics/btr244)

[5] Plummer, M. 2003. JAGS: A program for analysis of Bayesian graphical models using Gibbs sampling. *Proceedings of Workshop on Distributed Statistical Computing 2003*.

[6] Wabersich, D., Vandekerckhove, J. 2014. Extending JAGS: A tutorial on adding custom distributions to JAGS (with a diffusion model example). *Behavior Research Methods*. **46**, 15-28. (DOI: 10.3758/s13428-013-0369-3)

[7] Raftery, A.E., Lewis, S.M. 1992. One long run with diagnostics: Implementation strategies for Markov chain Monte Carlo. *Statistical Science*. **7**, 493-497. (DOI: doi:10.1214/ss/1177011143)

[8] Kass, R.E. & Raftery, A.E. 1995. Bayes factors. *JASA*. **90**, 773-795. (DOI: 10.1080/01621459.1995.10476572)

[9] Egilmez, N.K. & Jazwinski, S.M. 1989. Evidence for the involvement of a cytoplasmic factor in the aging of the yeast *Saccharomyces cerevisiae*. *J Bacteriol*. **171**, 37-42.

[10] Lee, S.S., Vizcarra, I.A., Huberts, D.H.E.W., Lee, L.P, & Heinemann, M. 2012. Whole lifespan microscopic observation of budding yeast aging through a microfluidic dissection platform. *Proc Natl Acad Sci*. **109**, 4916-4920. (DOI: 10.1073/pnas.1113505109)

[11] Clyde, M.A., Ghosh, J., & Littman, M.L. 2011. Bayesian adaptive sampling for variable selection and model averaging. *J Comput Graph Stat*. **20**, 80-101. (DOI: 10.1198/jcgs.2010.09049)

[12] Liang, F., Paulo, R., Molina, G., Clyde, M., Berger, J.O. 2008. Mixtures of g-priors for Bayesian variable selection. *JASA*. **103**, 410-423. (DOI: 10.1198/016214507000001337)

[13] Klugman, S.A., Panjer, H.H., & Willmot, G.E. *Loss Models: From Data to Decisions*. Wiley Press.

[14] Gelfand, A., & Ghosh, S. 1998. Model Choice: A Minimum Posterior Predictive Loss Approach. *Biometrika*. **85**, 1-11. (doi:10.1093/biomet/85.1.1)

[15] Vehtari, A., & Ojanen, J. 2012. A survey of Bayesian predictive methods for model assessment, selection and comparison. *Statist Surv*. **6**, 142-228. (doi:10.1214/12-SS102)